Polymer 116 (2017) 5–15

Contents lists available at ScienceDirect

Polymer

journal homepage: www.elsevier.com/locate/polymer

Methoxy group substitution on catechol ring of dopamine facilitates its polymerization and formation of surface coatings

Jieyu Zhang [a], Yong Shung Cheah [b], Sridhar Santhanakrishnan [b], Koon Gee Neoh [a, **], Christina L.L. Chai [b, *]

[a] Department of Chemical and Biomolecular Engineering, National University of Singapore, Kent Ridge, Singapore
[b] Department of Pharmacy, National University of Singapore, Kent Ridge, Singapore

ARTICLE INFO

Article history:
Received 19 November 2016
Received in revised form
15 March 2017
Accepted 22 March 2017
Available online 23 March 2017

Keywords:
Dopamine derivative
Surface modification
Silver nanoparticles
Antibacterial coating

ABSTRACT

Deposition of polydopamine on substrates is a facile and effective method of surface modification and the deposited polydopamine can reduce silver ions to form silver nanoparticles (AgNPs) for antibacterial applications. However, polydopamine deposition is a time-consuming process that usually requires 24 h to produce a dense surface coating. Since oxidation of dopamine is critical for its polymerization, we hypothesize herein that substitution of an electron-donating group on the catechol ring of dopamine can enhance its oxidation potential and subsequently accelerate its polymerization. In this work, dopamine substituted with a 5-methoxy group (OMeDA) was prepared. OMeDA polymerized faster than dopamine under similar reaction conditions, resulting in a polymer coating of 13 nm thickness on a silicon surface after 8 h, compared to the 24 h required for dopamine to form a coating of similar thickness. A polymer layer with AgNPs can be directly formed on the silicon substrate after exposure to a solution containing OMeDA and silver nitrate. After 2 h exposure, the silver content on the modified surfaces prepared with OMeDA was 187% higher than that obtained with dopamine, and the antibacterial efficacy of the former against *Staphylococcus aureus* was correspondingly higher than that of the latter. This study demonstrates that OMeDA with an electron-donating group in the catechol ring offers improvements over dopamine for surface modification applications.

1. Introduction

Surface modification confers new functionalities such as anti-corrosive, antibacterial and antifogging properties to existing materials, and has become an important field in materials science. A facile and effective method formulated in 2007 for modifying surfaces of nearly all types of organic and inorganic materials is via immersion of the substrates in a dopamine (DA) solution to form a polydopamine (PDA) layer. This method was inspired by observations that catechol and amine groups in the adhesive proteins secreted by mussels are able to attach to various surfaces [1]. The PDA layer formed by the polymerization of DA has excellent biocompatibility [2], which makes it particularly useful in biomedical applications.

The surface-immobilized PDA layer has an additional unique property in that it is able to form functional coatings containing metallic nanoparticles as PDA can readily reduce metal ions to metal nanoparticles which will subsequently bind to the catechol and amine groups of the PDA [3–6]. Some metallic nanoparticles (e.g. Ag and Cu) exhibit excellent antibacterial properties [7], and incorporation of these nanoparticles on surfaces using DA or PDA is a facile method for the fabrication of antibacterial surfaces which will have wide applications [8,9]. However, the preparation of antibacterial surfaces in this manner requires a relatively long processing time, typically 24 h to form a PDA layer of sufficient thickness to cover the surfaces [10–12], and this significantly limits its applications.

The formation of PDA is a complex redox process and a series of intermediates have been proposed to form during the polymerization process [13]. Although the detailed molecular mechanism is still under debate, the oxidation of DA is critical for its polymerization [13]. Substituents on the catechol ring of DA may affect its

* Corresponding author. Department of Pharmacy, National University of Singapore, 18 Science Drive 4, 117543, Singapore.
** Corresponding author. Blk E5, 4 Engineering Drive 4, #02-34, 117576, Singapore.
E-mail addresses: chenkg@nus.edu.sg (K.G. Neoh), phacllc@nus.edu.sg (C.L.L. Chai).

http://dx.doi.org/10.1016/j.polymer.2017.03.061
0032-3861/

redox properties, and polymerization of selected DA derivatives have been investigated [14–16]. For example, DA derivatives with electron-withdrawing groups such as -NO_2 [15] and -Cl [16] groups have lower oxidation potentials and polymerization rates as compared to DA [16]. This suggests that the introduction of an electron-donating group on the catechol ring of DA should increase its susceptibility to oxidation, and the rate of polymerization and deposition should be accelerated. It may also be possible to use the DA derivative with an electron-donating group for incorporating silver nanoparticles (AgNPs) for applications as antibacterial coatings. Polymerization of 5-hydroxyl substituted dopamine for surface modification has been reported [17], but to the best of our knowledge, the possibility that an electron-donating group on the catechol ring can accelerate the polymerization of DA derivatives has not been investigated. To verify these hypotheses, the polymerization of DA and 5-methoxy DA (OMeDA), as well as their applications in surface modification and AgNP deposition were investigated and compared.

2. Experimental section

2.1. Materials

Silicon (Si) wafers were obtained from Mitsubishi Silicon America, USA. Tris was obtained from Vivantis Technologies, Singapore. Deuterium oxide and Tris-d_{11} were purchased from Cambridge Isotope Laboratories, USA. *Staphylococcus aureus* (*S. aureus)* 25923 was purchased from American Type Culture Collection (Manassas, VA). All other chemicals, if not specified, were purchased from Sigma-Aldrich.

2.2. Synthesis of OMeDA

2.2.1. General experimental procedures

Thin layer chromatography was performed on precoated silica gel plates (Merck, Singapore) and visualized with UV light irradiation. Compounds **2**, **3** and **4** (in Scheme 1a) were purified by flash chromatography on a column using Merck silica gel 60 (230–400 mesh) or reversed-phase preparative chromatography using a RediSep Rf Gold® C18Aq column attached to a Sepacore® flash X10 system. Low-resolution electrospray ionization mass spectra (LRESIMS) were recorded on an Applied Biosystems MDS SCIEX API 2000 mass spectrometer. High resolution mass spectra (HRMS) were recorded on an Agilent mass spectrometer (electrospray ionization (ESI)-time of flight). Melting points (mp) were determined using a SRS OptiMelt MPA100 mp apparatus. Nuclear magnetic resonance (NMR) spectra were recorded on a Bruker spectrometer (Avance III 400 MHz) at 400 MHz for ^{1}H and 100 MHz for ^{13}C using chloroform-d, methanol-d_4 or dimethyl sulfoxide (DMSO)-d_6 as solvent. The chemical shifts are given in ppm, using the proton solvent residue signal ($CDCl_3$: δ 7.26, CD_3OD: δ 3.31, $(CD_3)_2SO$: 2.50) as a reference in the ^{1}H NMR spectra. The deuterium coupled signal of the solvent ($CDCl_3$: δ 77.16, CD_3OD: δ 49.00, $(CD_3)_2SO$: 39.52) was used as a reference in ^{13}C NMR spectra. The following abbreviations were used to describe the signals: s = singlet, d = doublet, t = triplet, m = multiplet and q = quartet.

The synthetic route to OMeDA is shown in Scheme 1a, and described below:

2.2.2. Synthesis of 3,4-dihydroxy-5-methoxybenzaldehyde (compound 2)

To a suspension of 5-bromovanillin (**1**, 9.2 g, 38.4 mmol) and NaOH (15.4 g, 384.8 mmol) in degassed water (400 mL), was added Cu powder (123 mg, 1.92 mmol) at room temperature (RT). The reaction mixture was refluxed for 60 h and then cooled down to RT. Na_2HPO_4 (273 mg, 1.92 mmol) was added to the reaction mixture and refluxed for 1 h. The reaction mixture was subsequently filtered and the filtered solid was rinsed with water. The filtrate collected was acidified with 6 N HCl until acidic. The resulting mixture was evaporated at 60 °C under reduced pressure (30 mmHg) until a thick slurry remained. The slurry was dissolved in ethyl acetate (500 mL), then dried with $MgSO_4$, filtered and evaporated. The crude residue was purified by flash chromatography (5% MeOH/DCM) to give compound **2** (6 g, yield of 90%) as a light brown solid [18] with mp 131–133 °C. ^{1}H NMR (400 MHz, $CDCl_3$): δ 9.79 (s, 1H), 7.14 (d, J = 1.7 Hz, 1H), 7.08 (d, J = 1.7 Hz, 1H), 3.97 (s, 3H). ^{13}C NMR (101 MHz, DMSO) δ 191.3, 148.5, 145.9, 141.1, 127.4, 110.9, 105.0, 56.0. ESI-MS: m/z 167.3 for $C_8H_9O_4$ ($[M - H]^-$, calculated m/z 167.0).

2.2.3. Synthesis of (E)-(((3-methoxy-5-(2-nitrovinyl)-1,2-phenylene)bis(oxy)) bis(methylene))dibenzene (compound 3)

Benzyl bromide (7.73 mL, 65.0 mmol) and potassium iodide (1.29 g, 7.78 mmol) were subsequently added to a suspension of compound **2** (4.37 g, 26.0 mmol) and K_2CO_3 (17.96 g, 130.0 mmol) in *N*,*N*-dimethylformamide (DMF) under nitrogen. The reaction mixture was heated at 80 °C for 4 h, and then cooled to RT followed by the removal of K_2CO_3 by filtration. The mixture was subsequently extracted with 500 mL of ethyl acetate and washed with 1 N HCl and brine. The crude product was dried over anhydrous Na_2SO_4, and the solvent was removed under reduced pressure. The product (9.15 g, 26.3 mmol) and ammonium acetate (6.07 g, 78.7 mmol) were dissolved in acetic acid, and nitromethane (7.09 mL, 131.3 mmol) was added to the reaction mixture. The reaction mixture was refluxed for 5 h, cooled to RT and then poured into water. The aqueous phase was extracted three times with 200 mL ethyl acetate. The combined organic phases were washed with brine (200 mL), dried over anhydrous Na_2SO_4, and concentrated under reduced pressure. The residue was subjected to flash chromatography (50% dichloromethane/petroleum ether) to give compound **3** (8 g, yield of 79%) with mp 126–128 °C. ^{1}H NMR (400 MHz, $CDCl_3$) δ 7.89 (d, J = 13.5 Hz, 1H), 7.48 (d, J = 13.5 Hz, 1H), 7.45–7.27 (m, 10H), 6.79 (d, J = 2.0 Hz, 1H), 6.75 (d, J = 2.0 Hz, 1H), 5.12 (s, 4H), 3.88 (s, 3H). ^{13}C NMR (101 MHz, $CDCl_3$) δ 154.4, 153.2, 141.5, 139.4, 137.4, 136.5 (2C), 128.8 (2C), 128.6 (2C), 128.4 (2C), 128.3, 128.2, 127.5 (2C), 125.5, 108.9, 106.8, 75.4, 71.6, 56.5. HRMS: m/z 392.1500 for $C_{23}H_{22}NO_5$ ($[M + H]^+$, calculated m/z 392.1492).

2.3. Synthesis of OMeDA

Palladium on carbon (10%, 1 g) and 6 N HCl (1.0 mL) were added to a suspension of compound **3** (1 g, 2.55 mmol) in a solution of ethanol and tetrahydrofuran (1:1) under nitrogen in a glass vessel. The vessel was flushed with hydrogen gas and pressurized to 345 kPa. The reaction mixture was stirred at RT for 15 min following which the hydrogen gas was removed by bubbling nitrogen gas through the mixture. The reaction mixture was then filtered through celite and the filtrate was concentrated under reduced pressure. The residue was purified by reversed-phase chromatography (95% H_2O/methanol) to produce OMeDA (compound **4**, 250 mg, 45%) as a pale brown solid with mp 190–192 °C. ^{1}H NMR (400 MHz, CD_3OD) spectrum: δ 6.41 (d, J = 1.9 Hz, 1H), 6.38 (d, J = 1.9 Hz, 1H), 3.84 (s, 3H), 3.12 (t, 2H), 2.81 (t, 2H). ^{13}C NMR (101 MHz, CD_3OD) spectrum: δ 150.0, 146.7, 134.1, 128.5, 110.3, 105.2, 56.7, 42.3, 34.3. HRMS: m/z 184.1 for $C_9H_{14}NO_3$ ($[M + H]^+$, calculated m/z 184.1).

2.4. Polymerization of OMeDA or DA in solution

DA or OMeDA (0.3 mM) was dissolved in Tris buffer (10 mM, pH 8.5), and the reaction mixture was incubated at 37 °C with shaking

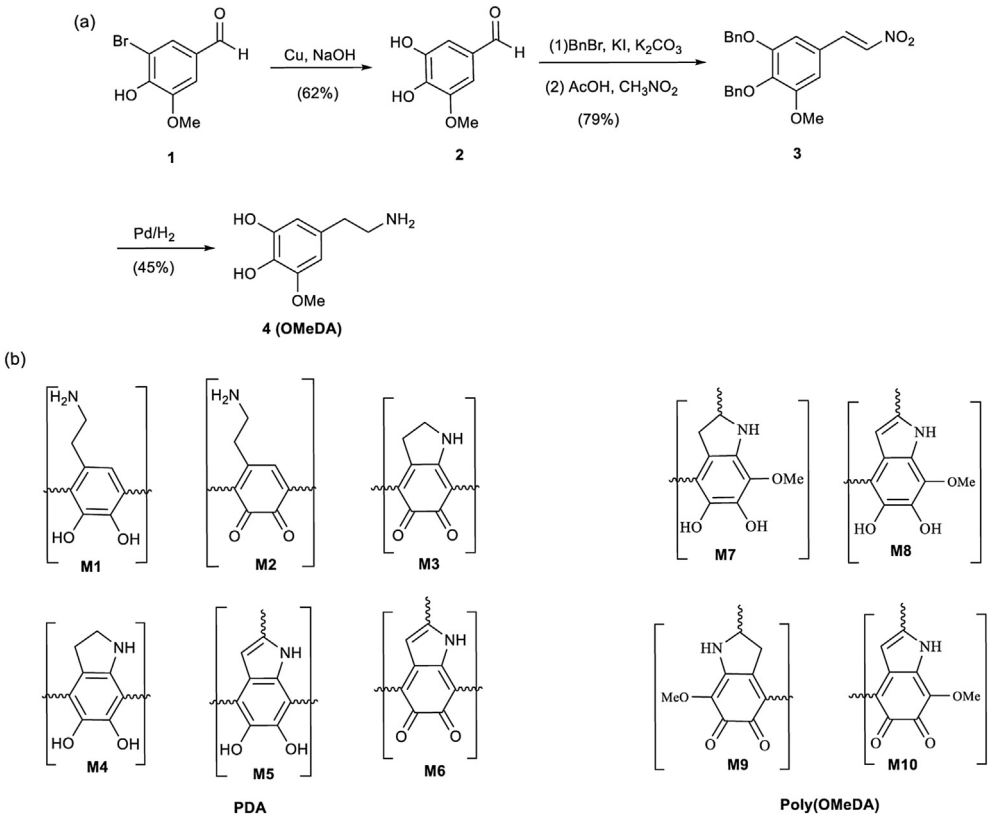

Scheme 1. **(a)** Synthetic procedure and structure of OMeDA. **(b)** Proposed major structural units of PDA and poly(OMeDA).

at 150 rpm over 24 h. At different time points (0, 2, 4, 8, 16 and 24 h), the UV-Vis absorbance spectrum (200–800 nm) of the solution was measured using a Shimadzu UV-1601 spectrophotometer with Tris buffer as the reference. Tris buffer was also used for baseline correction prior to measurement. The absorbance of the solution at 360 nm (A_{360}) was also continuously recorded over 4 h using a microplate reader (Tecan GENios, Switzerland). The progress of polymerization of DA and OMeDA were also monitored using NMR spectroscopy. DA or OMeDA (10.5 mM) was dissolved in Tris-d_{11} buffer (10 mM, pH 8.5) containing 1.75 mM DMSO as an internal standard. The solution was incubated at 37 °C with shaking at 150 rpm over 24 h. At predetermined time points (0, 2, 4, 8, 16 and 24 h), ^{1}H-NMR analysis of the samples was carried out on a Bruker Avance III spectrometer at 400 MHz.

PDA or polymer of OMeDA (poly(OMeDA)) obtained after polymerization of the respective monomer (10.5 mM) for 24 h in Tris buffer as mentioned above was collected by centrifuging the reaction mixture at 21,000×*g* for 30 min. The polymers were resuspended in deionized (DI) water and centrifuged for 3 cycles to remove the soluble residues, and then freeze-dried for 48 h. The Fourier transform infrared (FT-IR) spectra of the polymers were obtained in transmission mode using an Alpha Platinum-ATR FT-IR spectrophotometer (Bruker, Singapore) under ambient conditions. Solid-state ^{13}C NMR spectra were acquired at 100.61 MHz on a Bruker DRX 400 spectrometer (Bruker, Singapore) equipped with a 4 mm cross polarization-magic angle spinning (CP-MAS) probe. The contact time was set to 2 ms. The spectra were obtained after 800 scans at a spinning speed of 5 kHz for PDA, and 11541 scans at 8 kHz for poly(OMeDA). Thermogravimetric analysis (TGA) was conducted using a DTG-60AH analyzer (Shimadzu, Japan) at a heating rate of 5 °C/min in nitrogen atmosphere. Differential scanning calorimetry (DSC) was carried out with a DSC822e apparatus (Mettler Toledo, Switzerland) at a heating rate of 10 °C/min in nitrogen atmosphere.

2.5. Surface modification of Si with OMeDA and DA

Si wafers (0.725 mm thick) were cut into 1 × 1 cm^2 squares, and washed with a solution of 4.8% HF and 7% HNO_3 in water, and then cleaned ultrasonically in DI water and ethanol for 10 min each. After drying in air, each substrate was placed in one well of a 24-well plate followed by addition of 1.5 mL of 10.5 mM DA or OMeDA in Tris buffer. The reaction was carried out for different periods of time at 37 °C under continuous shaking at 150 rpm, and the substrates were then washed thoroughly with DI water and ethanol, and dried in air. The substrates are denoted as DA*x*h and OMeDA*x*h to indicate Si substrates incubated in DA and OMeDA solution for *x* h, respectively.

2.6. Deposition of AgNPs on Si surfaces

The Si substrates coated with PDA or poly(OMeDA) as mentioned above were immersed in 1.5 mL of 50 mM $AgNO_3$ aqueous solution at 37 °C with shaking at 150 rpm for 2, 4, 6, 24 or 48 h. After that, the substrates were washed thoroughly with DI water and ethanol, and dried in air. This process of AgNP immobilization is referred to as the "two-step method" in this study. The obtained substrates are denoted as DA*x*hAg*y*h and OMeDA*x*hAg*y*h which indicate the Si substrates were incubated in DA and OMeDA solution for *x* h followed by incubation in Ag^+ solution for *y* h.

For the "one-pot method" of AgNP immobilization, each Si substrate was immersed in 1.5 mL of freshly prepared solution containing 10.5 mM DA or OMeDA, and 50 mM $AgNO_3$ in Tris buffer. The reaction was carried out at 37 °C with shaking at 150 rpm for

2 h. After that, the substrates were washed thoroughly with DI water and ethanol, and dried in air. The obtained substrates prepared by the one-pot method using DA and OMeDA are denoted as DA/Ag2h and OMeDA/Ag2h substrates, respectively.

UV-Vis absorption spectroscopy was used to monitor the formation of AgNPs in solution. OMeDA or DA (40 μM), $AgNO_3$ (160 μM), and NaOH (1 mM) were added in DI water and the reaction was carried out for 2 h. The UV-Vis absorbance spectra (200–800 nm) of the resultant solution were recorded at 1 min intervals. NaOH aqueous solution was used as the reference and also for baseline correction prior to measurement.

2.7. Surface characterization

X-ray photoelectron spectroscopy (XPS) analysis was conducted on a Kratos AXIS Ultra DLD spectrometer (Kratos, UK) with a monochromatized Al Kα X-ray source (1486.7 eV photons). The binding energy was calibrated based on the C 1s peak at 284.6 eV. The PDA or poly(OMeDA)-coated Si surfaces were gently scratched with a scalpel, and atomic force microscopy (AFM; Bruker Dimension ICON, USA) was used to estimate the thickness of the coating layer. The surface morphology of the substrates was observed using field emission scanning electron microscopy (FESEM, FEI QUANTA 650 FEG, USA). The Ag content on the substrate was measured using inductively coupled plasma-mass spectroscopy (ICP-MS). Each substrate was immersed in 1 mL of 50% (v/v) nitric acid and incubated at 80 °C with shaking for 1 h to digest the Ag deposits. The supernatants were collected, and the Ag concentration in the solution was measured using a HP 7500A ICP-MS system (Agilent Technologies, USA). To investigate the possible release of surface Ag, each Ag-containing substrate was incubated in 1 mL of phosphate buffered saline (PBS) for 7 days, and the PBS was then collected and analyzed by ICP-MS.

2.8. Antibacterial effect of surface coating containing AgNPs

S. aureus was cultured at 37 °C overnight in tryptic soy broth, and then harvested by centrifugation at 2700 rpm for 10 min. The bacterial cells were resuspended in PBS at a concentration of 1×10^8 colony forming unit (CFU)/mL as estimated from the absorbance of the bacterial suspension. Absorbance at 600 nm (A_{600}) of 0.1 is equivalent to ~10^8 CFU/mL based on calibration from spread plate counting. The pristine and functionalized Si substrates were placed in a 24-well microplate, and 1 mL of bacterial suspension in PBS (1×10^8 CFU/mL) was added to each well followed by incubation at 37 °C for 4 h. The bacterial suspension was then removed, and the substrates were gently washed three times with PBS.

The viability of adherent bacteria on the substrates was assessed using a LIVE/DEAD Baclight™ bacterial viability kit (Life Technologies, USA) according to the manufacturer's instructions. Briefly, the bacterial cells on each substrate were stained with 50 μL of the combination dye provided with the kit in the dark for 15 min at RT, and then imaged using fluorescence microscopy (Leica, DM IL LED, USA).

The number of viable bacteria was quantified using the spread plate method as described in the literature [19]. Briefly, each substrate with adherent bacteria was immersed in 2 mL of PBS and sonicated for 7 min followed by 30 s of vortexing, to suspend the adherent bacteria in PBS. The bacterial suspension was then serially diluted, and 100 μL of each dilution was spread onto a nutrient agar plate followed by incubation overnight at 37 °C for determination of the number of viable bacteria.

2.9. Statistical analysis

For each condition and time point, at least three samples were used. One-way analysis of variance (ANOVA) with Tukey post-hoc

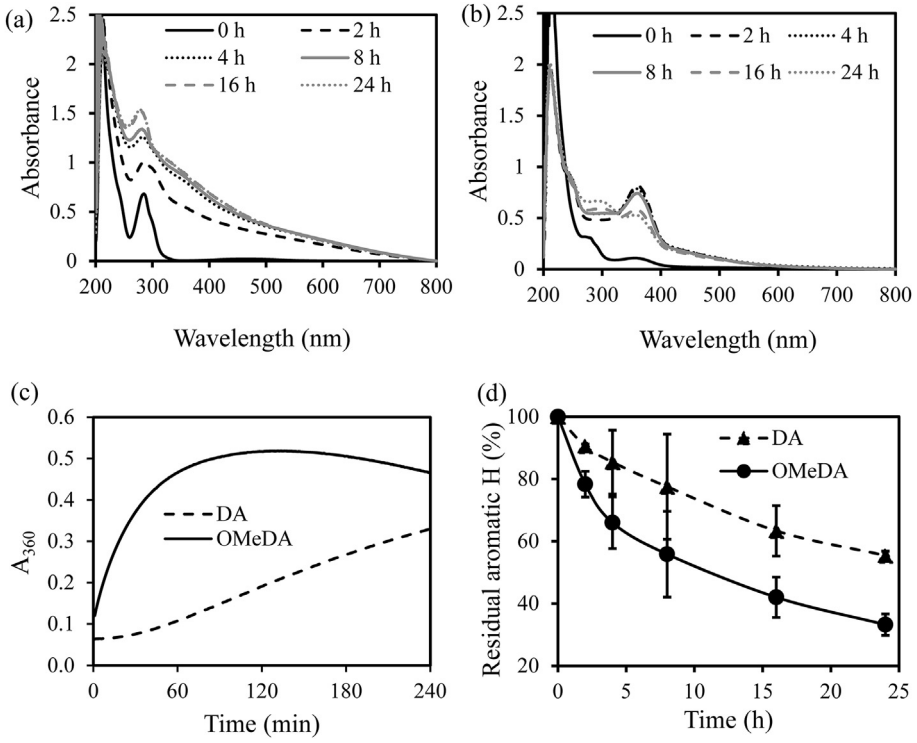

Fig. 1. UV-Vis spectra of the reaction mixture of **(a)** DA and **(b)** OMeDA polymerization in Tris buffer over 24 h **(c)** A_{360} over 4 h polymerization of DA and OMeDA in Tris buffer. **(d)** Percentage of residual aromatic H during polymerization of DA and OMeDA in Tris buffer.

test was used to evaluate the data and the results are reported as mean ± standard deviation. Statistical significance was accepted at $P < 0.05$.

3. Results and discussion

3.1. Synthesis of OMeDA

To synthesize OMeDA **4**, commercially available 5-bromovanillin (**1**) was first subjected to copper catalyzed hydroxylation to yield dihydroxy benzaldehyde **2** (Scheme 1a). O-Benzylation, followed by Henry reaction gave the nitro vinyl benzene derivative **3** with an overall yield of 79% over two steps. Subsequent treatment with palladium on carbon in the presence of hydrogen gas gave the desired 5-methoxydopamine **4** with a moderate yield of 45%.

3.2. Comparison of polymerization of OMeDA and DA in solution

The progress of the polymerization reaction of DA and OMeDA in solution was monitored using UV-Vis spectroscopy. Fig. 1a shows that as polymerization of DA progressed, the absorption at 360 nm increased presumably due to the formation of 5,6-dihydroxyindole, an intermediate in the oxidative polymerization reaction, which arises from intramolecular cyclization onto the quinone resulting from the initial oxidation step [20]. For OMeDA, an absorption peak at the same wavelength was also observed (Fig. 1b), suggesting that a compound/s possessing a similar structure/s was obtained. For both DA and OMeDA, the rate of increase in the absorption at 360 nm slowed after 4 h of reaction. In a subsequent experiment, A_{360} was continuously monitored using a microplate reader over the initial 4 h of polymerization. Fig. 1c shows that A_{360} of OMeDA increased at a faster rate than that of DA in the first 70 min of the polymerization reaction, suggesting a faster polymerization rate for OMeDA.

These observations were also confirmed from ^{1}H NMR spectroscopy used to monitor the progress of polymerization. In a typical experiment, DA or OMeDA was dissolved in deuterated Tris buffer containing DMSO as an internal standard, and the ^{1}H NMR spectra were recorded at different time points for the disappearance of the aromatic hydrogens signals due to DA or OMeDA respectively. Fig. 1d shows that during the polymerization of OMeDA and DA, the loss of aromatic signals attributable to OMeDA was faster than that of DA suggesting that OMeDA polymerized faster than DA. The faster rate of polymerization of OMeDA compared to DA may be attributed to the presence of the electron-donating -OMe group on the catechol ring which enhances its oxidation potential and facilitates the formation of the quinone intermediate [14].

To investigate the structural difference between PDA and poly(OMeDA), the polymers were analyzed using FT-IR absorption spectroscopy, solid-state NMR, TGA and DSC. As shown in Fig. 2a, the absorption bands at 1081, 1207 and 1283 cm^{-1} were attributed to C-O asymmetric stretching and bending vibrations [21]. The bands at 1354 cm^{-1} and 1456 cm^{-1} were assigned to the stretching vibrations of C-N-C and -C=N of indole rings [22]. The bands at 1508 and 1606 cm^{-1} were ascribed to the scissoring vibration of N-H, and C=C resonance vibration in the aromatic ring, respectively [21]. These results support the proposed structure of PDA reported in the literature, which contain the structural units with primary amino groups that do not undergo intramolecular cyclization (M1 and M2 in Scheme 1b) and indole-like moieties (indole and dihydroindoles) upon oxidation during polymerization (M3-6 in Scheme 1b) [23]. The band at 1606 cm^{-1} can serve as an internal reference for comparison of the FT-IR spectra of PDA and poly(OMeDA) since the aromatic rings are preserved during polymerization [13]. The FT-IR results show that relative to the band at 1606 cm^{-1}, the bands at 1354 and 1456 cm^{-1} were enhanced, and the band at 1508 cm^{-1} was reduced for poly(OMeDA) compared to PDA, which suggests that more indole-like moieties are present in poly(OMeDA) than in PDA [24].

In the ^{13}C NMR spectrum of PDA (Fig. 2b), signals at 30–50 ppm were assigned to aminoethyl moieties in the uncyclized units (M1 and M2) and carbon atoms of the saturated five-membered ring in M3 and M4 [25]. The catechol carbon (=C-OH) atoms in M1, M4, M5 (Scheme 1b) are observed at ~143 ppm [23]. Signals in the 110–130 ppm region were ascribed to the benzo carbon atoms of the aromatic ring [23]. The signals at 30–50 ppm in the ^{13}C spectrum of poly(OMeDA) are different from that of PDA. The peak at ~55 ppm was assigned to the carbon atom of the -OMe group [26], and this indicates that -OMe groups are still present in the structural units of poly(OMeDA). Since the FT-IR results (Fig. 2a) suggest less uncyclized moieties in poly(OMeDA) than in PDA and primary amino signals in the N 1s core-level XPS spectrum of poly(OMeDA) (Fig. 3c) were also nearly absent, it is likely that there are minimal uncyclized moieties in the poly(OMeDA). Therefore, the indole-like moieties (M7-10) which contain -OMe group in the catechol ring are proposed as the major structural units of poly(OMeDA) (Scheme 1b).

For both PDA and poly(OMeDA), the TGA data (Fig. 2b) shows

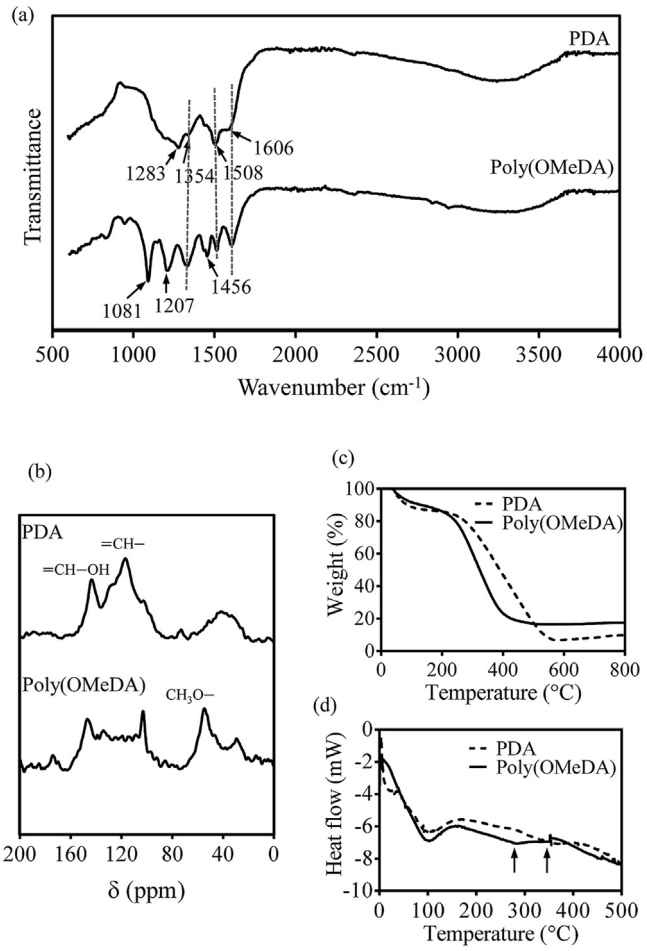

Fig. 2. **(a)** FT-IR spectra, **(b)** ^{13}C solid-state NMR spectra, **(c)** TGA, and **(d)** DSC scans of PDA and poly(OMeDA). The arrows in **(d)** indicate endothermic bands due to loss of water and polymer decomposition.

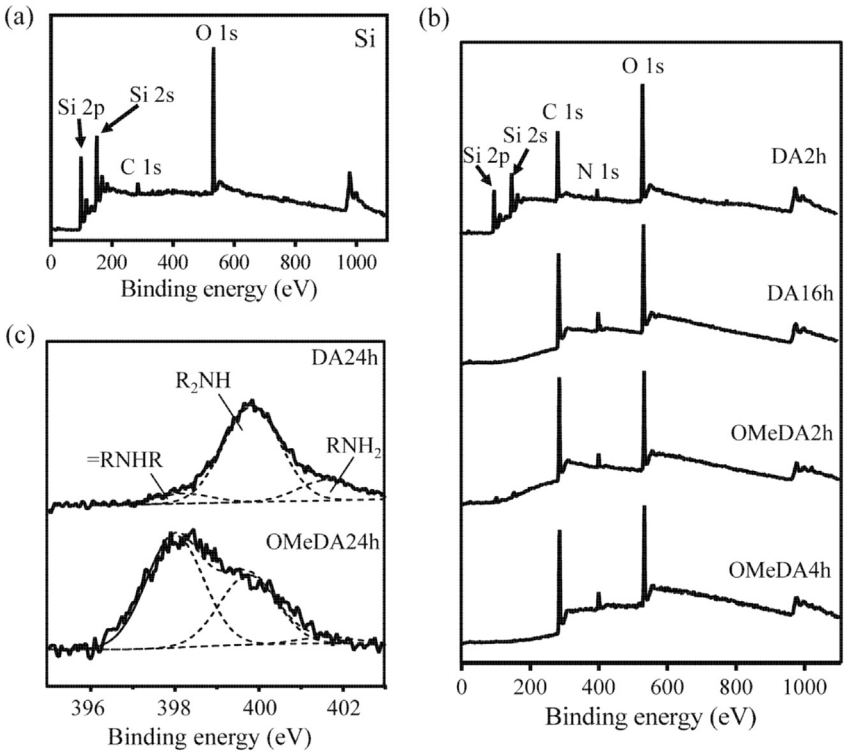

Fig. 3. XPS wide scan spectra of **(a)** pristine Si and **(b)** DA2h, DA16h, OMeDA2h and OMeDA4h substrates. **(c)** N 1s core-level spectra of DA24h and OMeDA24h substrates, respectively.

an initial weight loss upon heating from room temperature to 100 °C, which is attributed to the loss of water in the samples. The thermal degradation of PDA and poly(OMeDA) commenced at 267 and 207 °C, respectively, and poly(OMeDA) underwent a more rapid weight loss than PDA. The DSC results are shown in Fig. 2c. The endothermic event at 100 °C is due to evaporation of water, consistent with the weight loss observed in the TGA scans. The broad endothermic bands centered around 351 °C for PDA and 279 °C for poly(OMeDA) is associated with the decomposition of the polymers. The earlier onset of thermal degradation of poly(OMeDA) compared to PDA may be due to the higher electron density on the aromatic rings induced by the electron-donating -OMe groups, which increases the π-electron repulsion between the repeating units and decreases the polymer stability [27,28].

3.3. Surface modification of Si with OMeDA and DA

Since the above results have shown that OMeDA polymerized faster than DA in solution, OMeDA may require a shorter time than DA to form a polymer coating on a surface. To investigate this, Si substrates were placed in Tris buffer containing DA or OMeDA, and the changes in surface chemical composition with time were monitored by XPS. As shown in Fig. 3a, the pristine Si surface exhibited strong Si 2p and Si 2s signals. The Si surface after 2 h of exposure to DA shows a significant increase in C 1s signal and the appearance of N 1s signal (Fig. 3b), indicating successful deposition of PDA. However, the Si 2p and Si 2s signals remain strong suggesting that the deposited polymer did not fully cover the Si surface. When the reaction time was extended to 16 h, the Si surface was fully covered with PDA as indicated by the disappearance of Si signals in the XPS spectrum (Fig. 3b). In the case of OMeDA, the intensities of the Si 2p and Si 2s signals on the surface of the modified substrate were significantly reduced after 2 h of reaction (Fig. 3b). This result together with the increase in C 1s signal and presence of N 1s signal indicate that the deposited poly(OMeDA) has significantly covered the Si surface in just 2 h. After 4 h, the Si signals were no longer discernible (Fig. 3b), indicating that the surface was completely covered with poly(OMeDA). The shorter period of time needed for OMeDA to form a coating on the Si surface as compared to DA also suggests that OMeDA polymerized faster than DA, which is consistent with Fig. 1.

The surface composition of the polymers deposited on Si surfaces was analyzed using XPS. As shown in Fig. 3c, the N 1s peak can be fitted with three component peaks assigned to primary (RNH_2), secondary (R_2NH), and aromatic (=RNHR) amine species [21,29,30]. The primary amine is associated with uncyclized DA/OMeDA-like units present in the polymer, and the secondary and aromatic amine correspond to dihydroindole and indole moieties, respectively. Compared with PDA, poly(OMeDA) has a higher proportion of aromatic together with secondary amine moieties and a much lower proportion of primary amine functionalities (Fig. 3c). This suggests that the majority of OMeDA monomers underwent intramolecular cyclization during polymerization to result in more indole-like moieties in poly(OMeDA) than in PDA, consistent with the FT-IR and solid-state ^{13}C NMR spectra in Fig. 2.

To confirm that a shorter reaction time is needed for surface modification with OMeDA compared to DA, the thickness of the deposited polymer layer on Si was measured by AFM. As shown in Fig. 4, the thickness of the deposited polymer layer increased with increasing reaction time, and the deposited poly(OMeDA) layer was thicker than PDA under similar reaction conditions. Although the XPS results (Fig. 3a and b) indicated that most of the Si surface was covered with poly(OMeDA) after 2 h of reaction, the thickness of this polymer layer was too thin to be measured by AFM at this time point. After 24 h of reaction, a PDA layer with thickness of 12 ± 3 nm

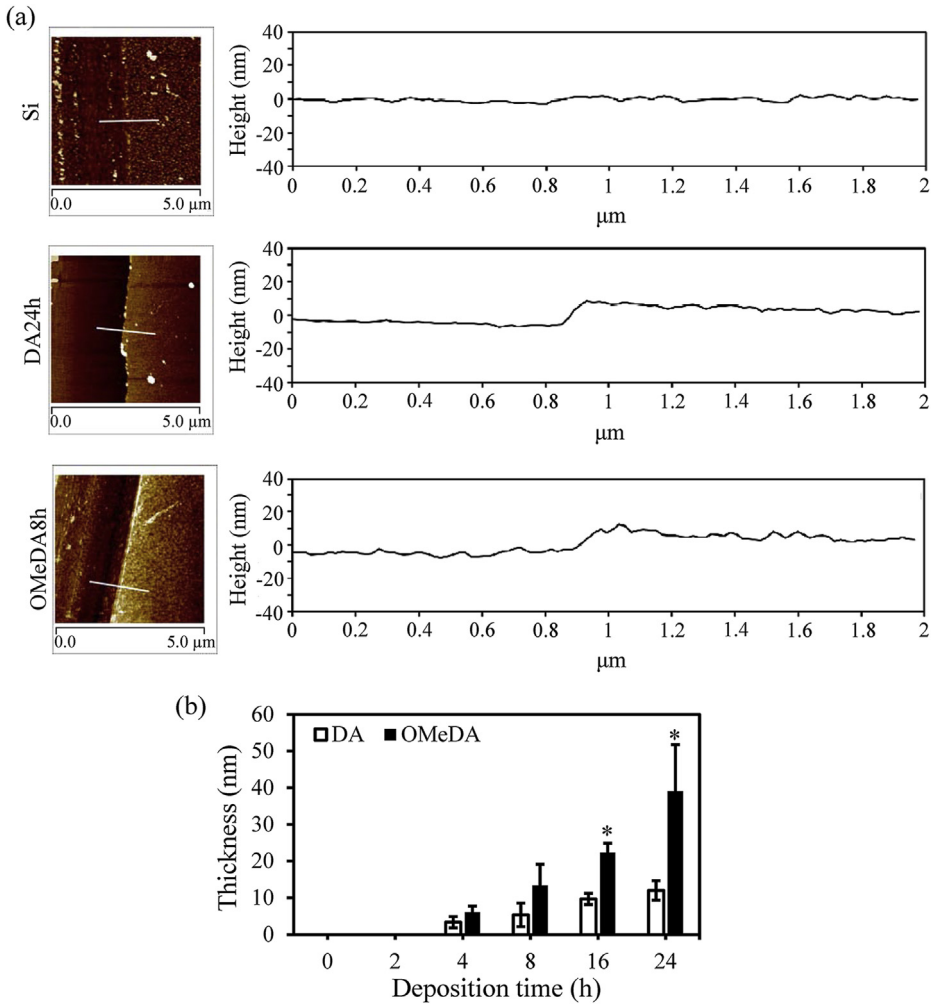

Fig. 4. **(a)** AFM images and surface profiles of pristine Si, DA24h, and OMeDA8h substrates. The white line in the AFM images indicates the location for surface profile measurement. **(b)** Thickness of PDA and poly(OMeDA) layer on Si substrates as a function of polymerization time.

was formed on Si, while a similar thickness of poly(OMeDA) was achieved in only 8 h (Fig. 4a). The thickness of poly(OMeDA) on Si was 39 ± 13 nm after 24 h, which was 225% thicker than that obtained with PDA over the same reaction period (Fig. 4b).

3.4. Deposition of AgNPs on Si surfaces using two-step method

The PDA and poly(OMeDA) deposited on Si surfaces were used to immobilize AgNPs for potential antibacterial applications. The DA24h and OMeDA8h substrates obtained by incubation of Si substrates in DA and OMeDA solution for 24 and 8 h, respectively, were chosen for comparison for their ability to reduce Ag^+ from solution and trap the formed AgNPs due to their similarity in coating thickness. The FESEM images of the DA24hAg2h and OMeDA8hAg2h substrates obtained by incubating the DA24h and OMeDA8h substrates in $AgNO_3$ solution for 2 h showed the presence of AgNPs on both substrates (Fig. 5). However, the size of the particles on the OMeDA8hAg2h substrate (Fig. 5e) was larger than those on the DA24hAg2h substrate (Fig. 5d). Quantitative ICP-MS analysis showed that the amount of Ag deposited on the OMeDA8h substrate was higher than on the DA24h substrate when the incubation time in the Ag^+ solution was shorter than 6 h (Fig. 5f). It is well-known that PDA exhibits inherent reductive capacity that results in Ag deposition upon exposure to its salt solutions without the need for an exogenous reducing agent [1]. The reduced Ag binds to the catechol and amine groups in PDA, and serves as seed for growth of nanoparticles [31]. The higher amount of Ag on the OMeDA8h substrate than on the DA24h substrate when the reaction time is less than 6 h indicates that poly(OMeDA) exhibits a higher reduction ability than PDA toward Ag^+. This is attributed to the electron-donating -OMe group in poly(OMeDA), which enhances its ability to reduce Ag^+. When the deposition time was extended to 24 h, the amounts of Ag deposited on the DA24h and OMeDA8h substrates were similar (Fig. 5f). This is likely due to the similarity in total reactive sites on the DA24h and OMeDA8h substrates since similar amounts of polymers were deposited on the surfaces as indicated by the similar thickness of the polymer layers (Fig. 4b). These reactive sites in the PDA and poly(OMeDA) layers for Ag^+ reduction were likely depleted by the excess Ag^+ in the reaction solution after 24 h since the Ag content on these substrates did not increase further when the deposition time was extended to 48 h.

The possible release of Ag from the DA24hAg2h and OMeDA8hAg2h substrates was investigated by incubating these substrates in PBS. The results show that only 1–2% of the Ag on the substrates was released after incubation in PBS for 7 days. This indicates that the AgNPs are strongly bound to the catechol groups in PDA and poly(OMeDA) on the Si surface [31].

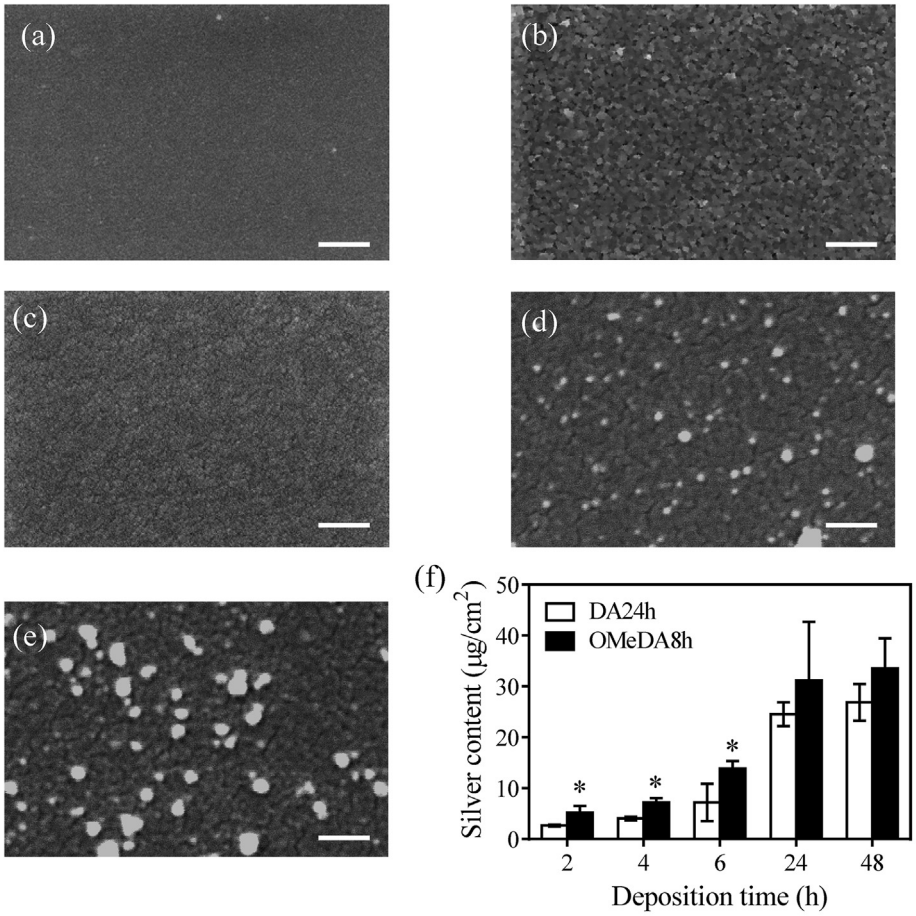

Fig. 5. (a–e) FESEM images of the surface of **(a)** pristine Si, **(b)** DA24h, **(c)** OMeDA8h, **(d)** DA24hAg2h, and **(e)** OMeDA8hAg2h substrates. Scale bar = 200 nm. **(f)** Silver content on the surfaces of DA24h and OMeDA8h substrates after incubation in $AgNO_3$ solution for different periods of time. * indicates significant difference ($P < 0.05$) compared with the results of DA24h over the same incubation period.

3.5. Deposition of AgNPs on Si surfaces using one-pot method

The two-step method for depositing AgNPs on Si requires a long processing time since more than 10 h was needed to prepare the OMeDA8hAg2h substrate, and more than 26 h to prepare the DA24hAg2h substrate. To shorten the processing time, the possibility of a one-pot method was investigated. When a Si substrate is incubated in a solution containing Ag^+ and DA or OMeDA, Ag^+ is expected to be reduced by DA or OMeDA to form AgNPs, and simultaneously, the oxidized monomers will polymerize and deposit on the Si surface together with the AgNPs. To test this hypothesis, the reduction of Ag^+ by DA and OMeDA in NaOH solution and the resultant AgNP formation was monitored using the absorbance at 410 nm which is the wavelength of surface plasmon absorption of AgNPs [32]. When OMeDA was used, AgNPs formed in greater quantity than DA under the same reaction condition as shown by the differences in surface plasmon absorption in Fig. 6a. These results are consistent with the UV-Vis absorption spectra in Fig. 1 which indicate that OMeDA polymerized faster than DA due to its higher oxidation potential.

The one-pot Ag deposition method was subsequently carried out by incubating Si substrates in the reaction medium containing DA or OMeDA and Ag^+. As shown in Fig. 6b, when OMeDA was used, the Si surface was more densely covered with AgNPs (the OMeDA/Ag2h substrate) compared to when DA was used (the DA/Ag2h substrate) after 2 h of reaction. The amount of Ag deposited after reaction with OMeDA was 187% higher than that with DA after 2 h of reaction (Fig. 6c). Comparison of the results in Figs. 6c and 5f shows that with the same time period for Ag^+ reduction (2 h), the amount of Ag on the DA/Ag2h and OMeDA/Ag2h substrates (from one-pot method) was much higher than that on the DA24hAg2h and OMeDA8hAg2h substrates (from two-step method). The release of the surface Ag on the substrates prepared by the one-pot method was tested, and the results show that only 1% of the surface Ag was released from the DA/Ag2h and OMeDA/Ag2h substrates after 7 days of incubation in PBS.

3.6. Antibacterial properties of AgNPs deposited on Si surface

Bacterial adhesion on a surface is the initial step for biofilm formation and subsequent infections. Therefore, inhibition of initial bacterial adhesion is critical for prevention of infections. In this study, *S. aureus* was selected as the target bacterium because it is the most prevalent causative pathogen of infections [33]. Different substrates with deposited AgNPs prepared using the two-step method (the DA24hAg2h and OMeDA8hAg2h substrates) or one-pot method (the DA/Ag2h and OMeDA/Ag2h substrates) were subjected to bacterial assay for comparison of their antibacterial property.

After incubation in *S. aureus* suspension in PBS for 4 h, the number of viable bacterial cells on the substrates without Ag (the DA24h, OMeDA8h, DA2h and OMeDA2h substrates) was not

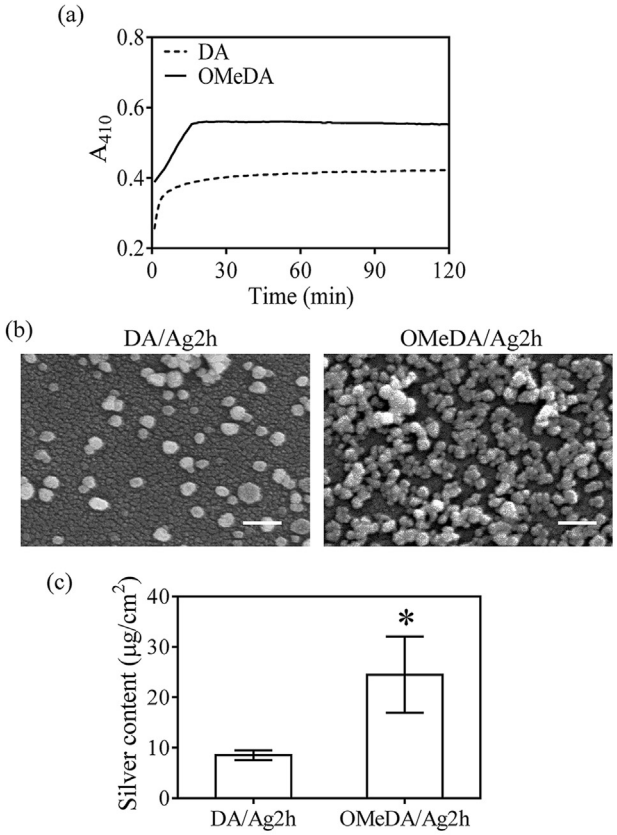

Fig. 6. **(a)** Absorbance of reaction mixture containing OMeDA or DA (40 μM), $AgNO_3$ (160 μM), and NaOH (1 mM) at 410 nm. **(b)** SEM images of DA/Ag2h and OMeDA/Ag2h substrates. Scale bar = 200 nm. **(c)** Quantification of amount of Ag deposited on the surfaces shown in **(b)**. * denotes significant difference ($P < 0.05$) compared with the result obtained with the DA/Ag2 substrate.

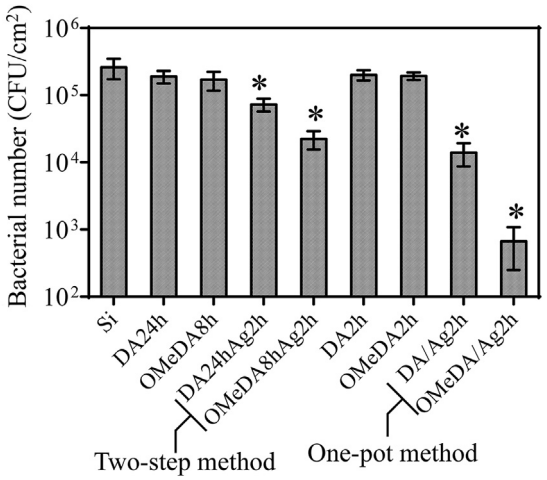

Fig. 7. Number of viable adherent *S. aureus* on pristine and modified Si substrates with or without deposited AgNPs after incubation in bacterial suspension (10^8 CFU/mL in PBS) for 4 h at 37 °C. * denotes significant difference ($P < 0.05$) compared with that on the pristine Si substrate.

significantly different from that on pristine Si (Fig. 7). This indicates that neither PDA nor poly(OMeDA) has antibacterial property. The number of viable *S. aureus* on the DA24hAg2h and OMeDA8hAg2h substrates decreased by 72% and 91%, respectively, as compared to that on pristine Si. For substrates prepared by the one-pot method,

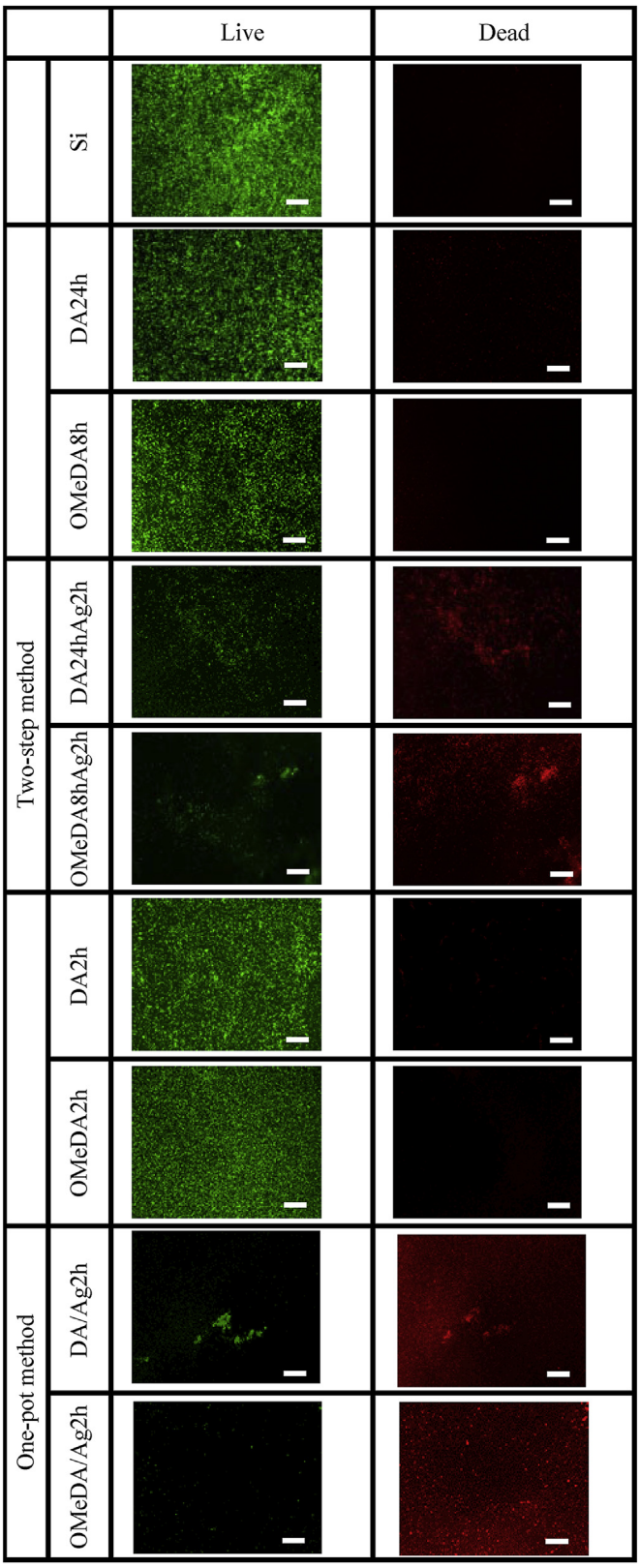

Fig. 8. Fluorescence microscopy images of *S. aureus* on pristine Si substrate, and modified Si substrates with or without deposited AgNPs after incubation in bacterial suspension (10^8 CFU/mL in PBS) for 4 h at 37 °C. Viable bacterial cells were stained green while membrane-compromised cells appeared red. (For interpretation of the references to colour in this figure legend, the reader is referred to the web version of this article.)

the number of viable *S. aureus* on the DA/Ag2h and OMeDA/Ag2h substrates decreased by 95% and over 2 orders of magnitude, respectively, compared to that on pristine Si.

To further investigate the antibacterial property of the Ag-containing surfaces, the bacteria on the substrates were subjected to live/dead staining, and the results are shown in Fig. 8. There were many live bacterial cells (stained green) but hardly any membrane-compromised bacterial cells (stained red) on pristine Si, and a similar observation was made for substrates without Ag (the DA24h, OMeDA8h, DA2h and OMeDA2h substrates). On the Ag-containing substrates (the DA24hAg2h, OMeDA8hAg2h, DA/Ag2h and OMeDA/Ag2h substrates), the number of live bacterial cells was much less than on pristine Si while the number of membrane-compromised cells increased significantly. These results illustrate the bactericidal effect of the AgNPs on the surface of the substrates. The mechanism by which AgNPs kill bacteria is not fully understood. AgNPs on the substrate can attach to bacterial surfaces and increase the permeability of cell walls and cell membranes, thereby adversely affecting the respiration process of bacterial cells [34]. Any AgNPs or Ag^+ ions released from the substrates can also enter the bacterial cells on the substrate and react with DNA and proteins, resulting in bacterial death [35]. The higher antibacterial efficacy of the OMeDA/Ag2h substrate compared to the other three Ag-containing surfaces is likely due to its higher content of AgNPs (Fig. 6c).

4. Conclusions

DA substituted with an electron-donating methoxy group (OMeDA) was shown to oxidize and polymerize more readily than DA. Similar to PDA, the poly(OMeDA) coating on Si surface can reduce Ag^+ to form AgNPs, but the reaction rate with poly(OMeDA) is higher than that of PDA of the same thickness. AgNP-containing coating can also be prepared using a one-pot method where the Si substrates were incubated in a solution containing Ag^+ and DA or OMeDA, and reduction of Ag^+ and polymerization of DA or OMeDA occur simultaneously. A distinct advantage of the one-pot method is that the processing time is much shorter than the two-step method. The amount of AgNPs deposited in the coating via the former (i.e. the DA/Ag2h and OMeDA/Ag2h substrates) after 2 h reaction time was higher than that achievable using the two-step method (i.e. the DA24hAg2h and OMeDA8hAg2h substrates) which requires more than 10 h. The AgNP-containing coating prepared using the one-pot method with OMeDA is strongly bactericidal, and most of the AgNPs on the OMeDA/Ag2h substrate are retained on the surface even after extended incubation in aqueous medium. Thus, this facile method is highly promising for fabricating antibacterial coatings.

Acknowledgments

We thank the Faculty of Science, National University of Singapore, SERC-A*STAR (Project no: 12212031) and National Medical Research Council of Singapore (Grant NMRC/BnB/12sep040) for financial support of this project.

References

[1] H. Lee, S.M. Dellatore, W.M. Miller, P.B. Messersmith, Mussel-inspired surface chemistry for multifunctional coatings, Science 318 (2007) 426–430.
[2] Y. Liu, K. Ai, J. Liu, M. Deng, Y. He, L. Lu, Dopamine-melanin colloidal nanospheres: an efficient near-infrared photothermal therapeutic agent for *in vivo* cancer therapy, Adv. Mater 25 (2013) 1353–1359.
[3] L. Tang, K.J.T. Livi, K.L. Chen, Polysulfone membranes modified with bioinspired polydopamine and silver nanoparticles formed *in situ* to mitigate biofouling, Environ. Sci. Technol. Lett. 2 (2015) 59–65.
[4] Y. Tan, G.X. Tan, C.Y. Ning, X.C. Rong, Y. Zhang, L. Zhou, Bioinspired polydopamine functionalization of titanium surface for silver nanoparticles immobilization with antibacterial property, J. Inorg. Mater 29 (2014) 1320–1326.
[5] Z.W. Guo, J.Z. Xue, T. Liu, X. Song, Y.Y. Shen, H.X. Wu, Antibacterial mechanisms of silica/polydopamine/silver nanoparticles against gram positive and gram negative bacteria, Micro Nano Lett. 9 (2014) 210–214.
[6] Z.S. Lu, J. Xiao, Y. Wang, M. Meng, *In situ* synthesis of silver nanoparticles uniformly distributed on polydopamine-coated silk fibers for antibacterial application, J. Colloid Interface Sci. 452 (2015) 8–14.
[7] F. Paladini, M. Pollini, A. Sannino, L. Ambrosio, Metal-based antibacterial substrates for biomedical applications, Biomacromolecules 16 (2015) 1873–1885.
[8] M.M. Mihai, A.M. Holban, C. Giurcaneanu, L.G. Popa, R.M. Oanea, V. Lazar, M.C. Chifiriuc, M. Popa, M.I. Popa, Microbial biofilms: impact on the pathogenesis of periodontitis, cystic fibrosis, chronic wounds and medical device-related infections, Curr. Top. Med. Chem. 15 (2015) 1552–1576.
[9] C. Brunon, E. Chadeau, N. Oulahal, C. Grossiord, L. Dubost, F. Bessueille, F. Simon, P. Degraeve, D. Leonard, Characterization of plasma enhanced chemical vapor deposition-physical vapor deposition transparent deposits on textiles to trigger various antimicrobial properties to food industry textiles, Thin Solid Films 519 (2011) 5838–5845.
[10] K. Lim, R.R.Y. Chua, B. Ho, P.A. Tambyah, K. Hadinoto, S.S.J. Leong, Development of a catheter functionalized by a polydopamine peptide coating with antimicrobial and antibiofilm properties, Acta Biomater. 15 (2015) 127–138.
[11] Y. Li, W. Yang, X. Li, X. Zhang, C. Wang, X. Meng, Y. Pei, X. Fan, P. Lan, C. Wang, X. Li, Z. Guo, Improving osteointegration and osteogenesis of three-dimensional porous Ti6Al4V scaffolds by polydopamine-assisted biomimetic hydroxyapatite coating, ACS Appl. Mater. Interfaces 7 (2015) 5715–5724.
[12] J. Jiang, L. Zhu, L. Zhu, H. Zhang, B. Zhu, Y. Xu, Antifouling and antimicrobial polymer membranes based on bioinspired polydopamine and strong hydrogen-bonded poly(N-vinyl pyrrolidone), ACS Appl. Mater. Interfaces 5 (2013) 12895–12904.
[13] J. Yang, M.A. Cohen Stuart, M. Kamperman, Jack of all trades: versatile catechol crosslinking mechanisms, Chem. Soc. Rev. 43 (2014) 8271–8298.
[14] J. Cui, J. Iturri, J. Paez, Z. Shafiq, C. Serrano, M. d'Ischia, A. del Campo, Dopamine-based coatings and hydrogels: toward substitution-related structure-property relationships, Macromol. Chem. Phys. 215 (2014) 2403–2413.
[15] Z. Shafiq, J. Cui, L. Pastor-Pérez, V. San Miguel, R.A. Gropeanu, C. Serrano, A. del Campo, Bioinspired underwater bonding and debonding on demand, Angew. Chem. Int. Ed. Engl. 51 (2012) 4332–4335.
[16] L. García-Fernández, J. Cui, C. Serrano, Z. Shafiq, R.A. Gropeanu, V.S. Miguel, J.I. Ramos, M. Wang, G.K. Auernhammer, S. Ritz, A.A. Golriz, R. Berger, M. Wagner, A. del Campo, Antibacterial strategies from the sea: polymer-bound Cl-catechols for prevention of biofilm formation, Adv. Mater 25 (2013) 529–533.
[17] S. Hong, J. Yeom, I.T. Song, S.M. Kang, H. Lee, H. Lee, Pyrogallol 2-aminoethane: a plant flavonoid-inspired molecule for material-independent surface chemistry, Adv. Mater. Interfaces 1 (2014) 1400113.
[18] A. Cervi, P. Aillard, N. Hazeri, L. Petit, C.L.L. Chai, A.C. Willis, M.G. Banwell, Total syntheses of the coumarin-containing natural products pimpinellin and fraxetin using Au(I)-catalyzed intramolecular hydroarylation (IMHA) chemistry, J. Org. Chem. 78 (2013) 9876–9882.
[19] J.Y. Zhang, K.G. Neoh, X.F. Hu, E.T. Kang, Mechanistic insights into response of *Staphylococcus aureus* to bioelectric effect on polypyrrole/chitosan film, Biomaterials 35 (2014) 7690–7698.
[20] K.W. Fan, J.J. Roberts, P.J. Martens, M.H. Stenzel, A.M. Granville, Copolymerization of an indazole ligand into the self-polymerization of dopamine for enhanced binding with metal ions, J. Mater. Chem. B 3 (2015) 7457–7465.
[21] R.A. Zangmeister, T.A. Morris, M.J. Tarlov, Characterization of polydopamine thin films deposited at short times by autoxidation of dopamine, Langmuir 29 (2013) 8619–8628.
[22] L. Lv, X. Wu, M. Li, L. Zong, Y. Chen, J. You, C. Li, Modulating $Zn(OH)_2$ rods by marine alginate for templates of hybrid tubes with catalytic and antimicrobial properties, ACS Sustain. Chem. Eng. 5 (2017) 862–868.
[23] J. Liebscher, R. Mrówczyński, H.A. Scheidt, C. Filip, N.D. Hădade, R. Turcu, A. Bende, S. Beck, Structure of polydopamine: a never-ending story? Langmuir 29 (2013) 10539–10548.
[24] R. Luo, L. Tang, S. Zhong, Z. Yang, J. Wang, Y. Weng, Q. Tu, C. Jiang, N. Huang, *In vitro* investigation of enhanced hemocompatibility and endothelial cell proliferation associated with quinone-rich polydopamine coating, ACS Appl. Mater Interfaces 5 (2013) 1704–1714.
[25] V. Proks, J. Brus, O. Pop-Georgievski, E. Večerníková, W. Wisniewski, J. Kotek, M. Urbanová, F. Rypáček, Thermal-induced transformation of polydopamine structures: an efficient route for the stabilization of the polydopamine surfaces, Macromol. Chem. Phys. 214 (2013) 499–507.
[26] U. Schenk, M. Hunger, J. Weitkamp, Characterization of basic guest compounds on solid catalysts by ^{13}C CP/MAS NMR spectroscopy of surface methoxy groups, Magn. Reson Chem. 37 (1999) S75–S78.
[27] T.M. Krygowski, M.A. Dobrowolski, K. Zborowski, M.K. Cyrański, Relation between the substituent effect and aromaticity. Part II. The case of meta- and para-homodisubstituted benzene derivatives, J. Phys. Org. Chem. 19 (2006) 889–895.
[28] C.A. Hunter, K.R. Lawson, J. Perkinsa, C.J. Urch, Aromatic interactions, J. Chem. Soc. Perkin Trans. 2 (5) (2001) 651–669.
[29] X. Han, L. Zhang, C. Li, Preparation of polydopamine-functionalized graphene-

Fe_3O_4 magnetic composites with high adsorption capacities, RSC Adv. 4 (2014) 30536–30541.
[30] A.S. Subramanian, J.N. Tey, L. Zhang, B.H. Ng, S. Roy, J. Wei, X.M. Hu, Synergistic bond strengthening in epoxy adhesives using polydopamine/MWCNT hybrids, Polymer 82 (2016) 285–294.
[31] T.S. Sileika, H.-D. Kim, P. Maniak, P.B. Messersmith, Antibacterial performance of polydopamine-modified polymer surfaces containing passive and active components, ACS Appl. Mater. Interfaces 3 (2011) 4602–4610.
[32] X. Wang, F. He, X. Zhu, F. Tang, L. Li, Hybrid silver nanoparticle/conjugated polyelectrolyte nanocomposites exhibiting controllable metal-enhanced fluorescence, Sci. Rep. 4 (2014) 4406.
[33] J.A. Inzana, E.M. Schwarz, S.L. Kates, H.A. Awad, Biomaterials approaches to treating implant-associated osteomyelitis, Biomaterials 81 (2016) 58–71.
[34] Z. Wang, J. Ou, Y. Wang, M. Xue, F. Wang, B. Pan, C. Li, W. Li, Anti-bacterial superhydrophobic silver on diverse substrates based on the mussel-inspired polydopamine, Surf. Coat. Technol. 280 (2015) 378–383.
[35] M.J. Hajipour, K.M. Fromm, A. Akbar Ashkarran, D. Jimenez de Aberasturi, I.R.d. Larramendi, T. Rojo, V. Serpooshan, W.J. Parak, M. Mahmoudi, Antibacterial properties of nanoparticles, Trends Biotechnol. 30 (2012) 499–511.